https://doi.org/10.5194/egusphere-2026-1884
Preprint. Discussion started: 26 May 2026

Development and evaluation of the ECHAM6-iMAPLE v1.0 coupled atmosphere-ecosystem model

Weijie Fu[1, †], Chenguang Tian[1, †], Yuan Zhao[1], Yihan Hu[1], Jingchao Huang[1], Haishan Chen[2], Xu Yue[1, *]

[1] State Key Laboratory of Climate System Prediction and Risk Management (CPRM), Jiangsu Collaborative Innovation Center of Atmospheric Environment and Equipment Technology, School of Environmental Science and Engineering, Nanjing University of Information Science & Technology (NUIST), Nanjing, 210044, China

[2] State Key Laboratory of Climate System Prediction and Risk Management (CPRM), Key Laboratory of Meteorological Disaster, Ministry of Education (KLME), Collaborative Innovation Center on Forecast and Evaluation of Meteorological Disasters (CIC-FEMD), School of Atmospheric Sciences, Nanjing University of Information Science and Technology, Nanjing, 210044, China

[*]**Correspondence:**
Xu Yue
(yuexu@nuist.edu.cn)

[†] These authors contributed equally to this work.

https://doi.org/10.5194/egusphere-2026-1884
Preprint. Discussion started: 26 May 2026

Abstract. Land-atmosphere interactions play a fundamental role in regulating climate variability, ecosystem productivity, and air quality through coupled exchanges of energy, water, carbon, and reactive trace gases. However, many Earth system models adopt simplified representations of vegetation physiological processes, leading to biases in terrestrial carbon and water fluxes and increased uncertainties in climate simulations. Here, we present ECHAM6-iMAPLE v1.0, a newly coupled modeling framework that integrates the interactive Model for Air Pollution and Land Ecosystems (iMAPLE v1.0) into the ECHAM6 atmospheric general circulation model. The coupled model is evaluated against reanalysis, benchmark, and satellite datasets. Compared with the original configuration, ECHAM6-iMAPLE substantially improves simulations of gross primary productivity, evapotranspiration, and leaf area index, capturing their spatial distributions and seasonal cycles more reasonably. These improvements arise from well-constrained physiological parameters calibrated using extensive site-level observations and a more realistic representation of key biophysical processes in iMAPLE. With improved carbon and water fluxes, simulations of soil temperature, soil moisture, and surface air temperature show reduced root mean square errors. Overall, evaluations demonstrate that ECHAM6-iMAPLE provides a useful tool for investigating atmosphere-ecosystem interactions and their implications for future climate change projections.

Keywords: ECHAM6, iMAPLE, ecosystem, atmosphere, interaction, coupling

https://doi.org/10.5194/egusphere-2026-1884
Preprint. Discussion started: 26 May 2026

1. Introduction

Terrestrial ecosystems and climate systems are tightly linked through exchanges of energy fluxes, water vapor, carbon, and trace gases, thereby regulating regional and global climate patterns (Pielke et al., 1998; Green et al., 2017). Climate conditions directly influence vegetation growth (Parmesan and Yohe, 2003; Fastovich et al., 2025), distribution (Seidl et al., 2017; Nolan et al., 2018), and phenology (Higgins et al., 2023), and atmospheric pollutants such as ozone can damage plant physiological processes by reducing photosynthetic rates and stomatal conductance (Sitch et al., 2007; Cao et al., 2024). Conversely, terrestrial ecosystems exert substantial feedbacks on the atmosphere through physical and biogeochemical processes (Bonan, 2008; Heimann and Reichstein, 2008). For instance, terrestrial vegetation absorbs approximately 120 Pg C/year through photosynthesis (Beer et al., 2010; Friedlingstein et al., 2025), while vegetation and soil respiration return a comparable amount of CO_2 into the atmosphere (Ruehr et al., 2023). Ecosystem also influences the partitioning of sensible and latent heat fluxes by modulating transpiration and canopy conductance (Williams and Torn, 2015; Zeng et al., 2017; Forzieri et al., 2020), thus affecting precipitation patterns and the intensity/frequency of hydrological extremes (Zhou et al., 2021; Schumacher et al., 2022; Zhang et al., 2025).

Models that couple atmospheric general circulation with vegetation dynamics provide essential tools for investigating interactions between the atmosphere and terrestrial ecosystems (Sellers et al., 1997; Berg et al., 2016). However, vegetation models differ substantially in their parameterization schemes for representing complex hydrological, biogeophysical, and biogeochemical processes. Uncertainties arising from these parameterization differences can propagate through land-atmosphere interactions, thereby influencing weather forecasts and climate projections (Wei et al., 2010; Wei et al., 2018). Despite continuous development, many widely used vegetation models still lack a comprehensive representation of key ecosystem processes that regulate land-atmosphere exchanges of energy, water, and biogeochemical constituents (Pitman, 2003; Blyth et al., 2021). For instance, vegetation dynamics such as seasonal variations of leaf area are usually prescribed with empirical parameters rather than being simulated through interactive responses to environmental drivers (Gulden et al., 2007; Niu et al., 2011; Fisher and Koven, 2020). This limitation constrains the ability of models to realistically capture ecosystem dynamics and their feedbacks to atmosphere.

https://doi.org/10.5194/egusphere-2026-1884
Preprint. Discussion started: 26 May 2026

In this study, we present the coupled atmosphere-ecosystem model ECHAM6-iMAPLE, developed by integrating the interactive Model for Air Pollution and Land Ecosystems (iMAPLE) v1.0 (Yue et al., 2024) into the atmospheric general circulation model ECHAM version 6.3 (https://redmine.hammoz.ethz.ch/projects/hammoz, last access: 30 March 2026) (Tegen et al., 2019). ECHAM6 has been extensively developed with multiple Earth system components and has participated in the Sixth Coupled Model Intercomparison Project (CMIP6) (Stevens et al., 2013; Sidorenko et al., 2015; Cao et al., 2018). The model has been widely used for global climate simulations and projections owing to the robust dynamical core and comprehensive physical parameterizations (Stevens et al., 2013; Siongco et al., 2017; Kretzschmar et al., 2019). iMAPLE is a global dynamic vegetation model designed to simulate plant growth and terrestrial carbon cycle interactively (Yue et al., 2024). It has demonstrated robust capability in simulating major carbon and water fluxes through its participation in the multi-model intercomparison project for Global Carbon Budget (Friedlingstein et al., 2025). Here, we evaluate the dynamically simulated carbon and water fluxes from ECHAM6-iMAPLE, and compare its performance with the original ECHAM6 model in representing critical surface variables, including soil temperature, soil moisture, near-surface air temperature, and precipitation. A detailed description of the model coupling framework is provided in Section 2. Section 3 presents the simulation results and model evaluations. Concluding remarks and future research perspectives are discussed in Section 4.

2. Models, methods, and data

2.1 Descriptions of iMAPLE

iMAPLE is an interactive model developed to investigate the interplay between air pollution and terrestrial ecosystems (Yue et al., 2024). The model evolved from version 1.0 of the Yale Interactive terrestrial Biosphere (YIBs) model, with an expanded focus on explicitly representing the interaction between atmospheric chemistry and land ecosystems (Yue and Unger, 2015). Compared to YIBs, iMAPLE incorporates several new processes, including dynamic fire emission (Pechony and Shindell, 2009; Li et al., 2012), wetland methane emissions (Walter et al., 2001; Zhu et al., 2014), and photosynthetic limitation under environmental stress (Arora et al., 2009). Furthermore, iMAPLE integrates the process-based hydrological scheme Noah-MP, which enables dynamical simulation of soil temperature and moisture and facilitates tight coupling

https://doi.org/10.5194/egusphere-2026-1884
Preprint. Discussion started: 26 May 2026

between the carbon and water cycles (Niu et al., 2011). These improvements substantially enhance the model's capacity to represent ecosystem-atmosphere interactions. Below, we briefly describe the parameterizations of vegetation biophysics and hydrological processes. A comprehensive model description is provided in Yue et al. (2024) and Niu et al. (2011).

2.1.1 Vegetation biophysics of iMAPLE

The vegetation biophysics in iMAPLE utilizes the canonical Michaelis–Menten enzyme-kinetics scheme to simulate photosynthetic processes for both C_3 and C_4 plant functional types (Farquhar et al., 1980; Von Caemmerer and Farquhar, 1981). The total leaf photosynthesis (A_{tot}, μmol m^{-2} [leaf] s^{-1}) is limited by one of three biochemical processes:

$$A_{tot} = min(J_c, J_e, J_s) \quad (1)$$

Here, J_c represents the Rubisco-limited rate of carbon fixation catalyzed by the enzyme ribulose 1,5-bisphosphate (RuBP) carboxylase/oxygenase (Rubisco). J_e denotes the RuBP regeneration-limited rate driven by electron transport through the Calvin cycle and associated thylakoid reactions. J_s is the limitation imposed by end-product synthesis, reflecting the capacity for starch and sucrose formation to regenerate inorganic phosphate required for photophosphorylation in C_3 plants, or phosphoenolpyruvate (PEP) regeneration in C_4 plants. The rates J_c, J_e, and J_s are parameterized as functions of environmental meteorological conditions and photosynthetic capacity, including the maximum carboxylation rate (V_{cmax}, μmol m^{-2} s^{-2}) (Collatz et al., 1991; Collatz et al., 1992a):

$$J_e = \begin{cases} a_{leaf} \times PAR \times \alpha \left(\frac{C_i - \Gamma_*}{C_i + 2\Gamma_*}\right) & for\ C3\ plant, \\ a_{leaf} \times PAR \times \alpha & for\ C4\ plant \end{cases} \quad (2)$$

$$J_c = \begin{cases} V_{cmax} \left(\frac{C_i - \Gamma_*}{C_i + K_c(1 + {O_i}/{K_o})}\right) & for\ C3\ plant, \\ V_{cmax} & \text{for C4 plant} \end{cases} \quad (3)$$

$$J_s = \begin{cases} 0.5V_{cmax} & for\ C3\ plant, \\ K_s \times V_{cmax} \times \frac{C_i}{P_s} & for\ C4\ plant \end{cases} \quad (4)$$

Here, Ci and O_i denote the partial pressures (Pa) of CO_2 and oxygen inside the leaf, while Γ_* (Pa) refers to the CO_2 compensation point. The Michaelis–Menten constants

https://doi.org/10.5194/egusphere-2026-1884
Preprint. Discussion started: 26 May 2026

for Rubisco carboxylation and oxygenation are represented by Kc (Pa) and Ko (Pa), respectively. PAR (μmol m^{-2} s^{-1}) denotes the incident photosynthetically active radiation, a_{leaf} is the light absorption coefficient of the leaf, and α represents the intrinsic quantum efficiency. P_s is the ambient pressure, and K_s is a constant with a value of 4000 (Lawrence et al., 2011). V_{cmax} is derived from its optimum value at 25 °C (V_{cmax25}) through a Q10 function.

The canopy radiative transfer scheme employs an adaptive approach, typically dividing vegetation into 2-16 vertical layers to resolve light stratification within the canopy. At each layer, a two-leaf approach further partitions leaf area into sunlit and shaded fractions, thereby capturing canopy light heterogeneity and distinguishing the different light-use efficiency under diffuse and direct radiation (Spitters, 1986; Spitters et al., 1986). Gross primary productivity (GPP) is then calculated by integrating photosynthesis across all canopy layers:

$$GPP = \int_0^{LAI} A_{tot} dL \quad (5)$$

After accounting for autotrophic respiration, net carbon assimilation is allocated to leaves, stems, and roots to support plant growth and leaf development. Leaf area index (LAI) is updated at 10-day intervals based on total leaf carbon and vegetation phenology.

2.1.2 Water cycle of iMAPLE

The hydrological cycle in iMAPLE adopts the Noah-MP module, which resolves the grid-scale water balance among precipitation (P, Kg m^{-2} s^{-1}), evapotranspiration (ET, Kg m^{-2} s^{-1}), runoff, and changes in terrestrial water storage (ΔTWS) at each grid:

$$P = \mathrm{ET} + \mathrm{runoff} + \Delta\mathrm{TWS} \quad (6)$$

ET is further divided into plant transpiration (E_{tr}), canopy evaporation (E_{can}), and ground evaporation (E_{gro}):

$$ET = E_{tr} + E_{can} + E_{gro} \quad (7)$$

The runoff comprises surface (R_{srf}) and subsurface (R_{sub}) parts:

$$runoff = R_{srf} + R_{sub} \quad (8)$$

Terrestrial water storage (TWS) encompasses three major components: groundwater storage (W_{gw}), which refers to water held in aquifers; soil water content (W_{soil}),

https://doi.org/10.5194/egusphere-2026-1884
Preprint. Discussion started: 26 May 2026

representing moisture within four soil layers (N_{soil}=4); and snow water equivalent (W_{snow}), indicating the liquid water equivalent of accumulated snowpack:

$$TWS = W_{gw} + W_{snow} + \sum_{i=1}^{N_{soil}=4} W_{soil} \quad (9)$$

2.2 Descriptions of ECHAM v6.3

ECHAM6 is the sixth generation of the ECHAM atmospheric general circulation model, developed by the Max Planck Institute for Meteorology (MPI-M) (Giorgetta et al., 2013; Stevens et al., 2013). Its dynamical core employs a hybrid numerical framework that combines spectral and finite-difference methods to solve the primitive equations (Arakawa, 1966; Bourke et al., 1977). Horizontally, ECHAM6 utilizes a truncated spherical harmonic expansion to calculate the nonlinear and parameterized terms of dynamical fields on a Gaussian grid. Vertically, the model employs a hybrid sigma-pressure coordinate system implemented on a Lorenz grid (Phillips, 1957; Simmons and Burridge, 1981).

Compared to previous ECHAM versions, ECHAM6 incorporates substantial improvement in key physical processes, including a more sophisticated representation of land surface processes, updated radiation parameterizations, refined surface albedo calculations, and revised convection triggering criteria (Stier et al., 2005; Crueger et al., 2018; Tegen et al., 2019). The model supports multiple configurations, with horizontal resolutions spanning from T31 (3.75°) to T255 (0.7°) and 47 or 95 vertical layers (Stevens et al., 2013). In this study, we adopt the T63L47 configuration to enable coupling with the iMAPLE model. The T63 spectral grid is characterized by an approximate grid spacing of 1.875° in longitude and latitude. The L47 vertical configuration comprises 47 layers extending from the surface to 0.01 hPa.

ECHAM6 employs JSBACH version 3.10 to simulate land vegetation processes (Goll et al., 2017). Compared to the earlier versions, JSBACH v3.10 incorporates a soil water diffusion scheme that provides a more physically consistent representation of terrestrial water budgets. In addition, modules for the dynamical simulation of LAI, canopy radiative transfer, and leaf-level photosynthesis have been integrated into the current versions. Here, we provide a brief description of JSBACH v3.10 to facilitate the comparisons of its physical processes with those of iMAPLE v1.0.

https://doi.org/10.5194/egusphere-2026-1884
Preprint. Discussion started: 26 May 2026

2.2.1 Vegetation biophysics of JSBACH

JSBACH utilizes a tiling scheme to represent land surface heterogeneity and incorporates dynamic vegetation components consisting of 12 plant functional types (PFTs) and two bare-ground classes (Reick et al., 2013). For vegetation productivity, JSBACH adopts parameterizations from the Biosphere Energy Transfer Hydrology (BETHY) module, including canopy radiative transfer calculations and two distinct photosynthesis simulations (Sellers et al., 1992; Knorr, 2000).

Leaf photosynthesis in BETHY is implemented in two sequential steps. First, potential productivity is calculated without considering soil water deficit, which generates stomatal conductance under unstressed conditions. The stomatal conductance derived in this step is then passed to the soil hydrological scheme to estimate potential transpiration and associated water loss. Second, stomatal conductance is adjusted according to soil water availability, and photosynthesis is recalculated to obtain actual productivity. The A_{tot} in JSBACH v3.10 can be expressed as:

$$A_{tot} = min(J_c,\ J_e) \tag{10}$$

In JSBACH, photosynthesis of C_3 plants is represented using the Farquhar model (Farquhar et al., 1980), consistent with iMAPLE. For C_4 plants, JSBACH utilizes the Collatz model (Collatz et al., 1992b). The primary difference between the Collatz and Farquhar formulations lies in their parameterization of the carboxylation rate (J_c) and the electron transport rate (J_e):

$$J_c = k * C_i \tag{11}$$

$$J_e = \frac{1}{2\theta_s}\left(V_{p,max} + J_i - \sqrt{\left(V_{p,max} + J_i\right)^2 - 4\theta_s * V_{p,max} * J_i}\right) \tag{12}$$

$$J_i = \alpha_i * I \tag{13}$$

$$I = \left(R(0) + R_{\downarrow}(0)\right) * fAPAR \tag{14}$$

Here k is specific parameters for carboxylase, C_i the partial pressures of CO_2 and oxygen inside the leaf (in Pa), θ_s is a curve parameter for J_e. $V_{p,max}$ is the maximum electron rate for C_4 plant. J_i is the rate of light-dependent potential electron transport. I is the radiation absorbed by leaves. α_i is the integrated C_4 quantum efficiency. $R(0)$ and $R_{\downarrow}(0)$ represent the direct radiation and downward diffuse radiation at the top of the canopy, respectively. $fAPAR$ is the fraction of absorbed *PAR*.

The canopy radiative transfer in JSABCH is based on a two-stream approximation (Meador and Weaver, 1980; Dickinson, 1983; Sellers et al., 1992). This approach

https://doi.org/10.5194/egusphere-2026-1884
Preprint. Discussion started: 26 May 2026

assumes (i) a uniform vertical distribution of leaves within the canopy, (ii) horizontal homogeneity in radiation fields, (iii) purely vertical radiative fluxes, and (iv) identical leaf reflectance and transmittance for direct and diffuse radiation across the entire PAR spectrum. For GPP calculation, the procedure is consistent with that applied in iMAPLE. In the second computational step, water-stressed photosynthetic rates are integrated across all canopy layers to obtain ecosystem productivity. LAI is dynamically simulated using the phenological model of LoGro-P (Dalmonech and Zaehle, 2013; Dalmonech et al., 2015).

2.2.2 Water cycle of JSBACH

The soil hydrology module in JSBACH discretizes the soil column into five layers extending to a depth of 10 meters (Hagemann and Stacke, 2015). Vertical soil water movement is described using the Richards equation, while surface runoff and drainage are calculated based on the Arno scheme (Richards, 1931; Todini, 1996). Transpiration is regulated through root-zone soil layers, and carbon-water coupling is implemented to represent interactions among hydrological and biogeochemical processes. The total soil water content $\partial h_{tot}^{(i)}$ of each tile (i) can be expressed as:

$$\rho_\omega \frac{\partial h_{tot}^{(i)}}{\partial t} = (1 - f_v)P - E_{bs}^{(i)} - E_{tr}^{(i)} + M_{sn}^{(i)} + M_{snc}^{(i)} - R_{srf}^{(i)} - R_d^{(i)} \quad (15)$$

where ρ_ω denotes the density of water. f_v represents the fraction of precipitation (P) intercepted by the canopy, E_{bs} is bare soil evaporation, and E_{tr} denotes transpiration. M_{sn} and M_{snc} represent snowmelt at the surface and within the canopy, respectively. R_{srf} is surface runoff and R_d is subsurface drainage.

2.3 Coupling between ECHAM6 and iMAPLE

Although both JSBACH and iMAPLE participated in the multi-model intercomparison project for Global Carbon Budget, iMAPLE demonstrated superior performance relative to JSBACH in simulating key carbon (e.g., GPP) and water (e.g., ET) fluxes (Friedlingstein et al., 2025). In addition, iMAPLE incorporates a more comprehensive representation of biogeochemical processes, thereby enhancing the simulation of interactions between atmospheric chemistry and terrestrial ecosystems. In this study, iMAPLE was coupled to the ECHAM6 global circulation model (Fig. 1)

https://doi.org/10.5194/egusphere-2026-1884
Preprint. Discussion started: 26 May 2026

and configured to run in parallel with JSBACH, enabling a systematic comparison of their process representations and model performance.

ECHAM6 integrates atmospheric dynamic processes at an interval of 7.5 minutes, which is much shorter than the 60-minute interval used in iMAPLE. As a result, simulated climatic variables from ECHAM6 are passed to iMAPLE every 8 ECHAM6 time steps. To ensure seamless information exchange, iMAPLE adopts the same core functional modules as ECHAM6 for input/output (I/O) operations, memory management, parallel computation, and calendar handling. At each coupling interval, ECHAM6 provides hourly meteorological variables to iMAPLE, including precipitation, surface air temperature, wind speed, humidity, surface pressure, CO_2 concentrations, direct and total radiation. In return, iMAPLE feeds back simulated soil temperature, soil moisture, and *ET* to ECHAM6, thereby affecting the land surface energy balance and atmospheric general circulation. Extensive numerical tests were conducted to ensure integration stability and computational efficiency of the coupled modeling framework.

The land cover dataset used in iMAPLE was developed by integrating satellite-based observations from Moderate Resolution Imaging Spectroradiometer (MODIS) and Advanced Very High Resolution Radiometer (AVHRR) (Defries et al., 2000; Hansen et al., 2003), which include nine PFTs representing major global terrestrial ecosystems. In contrast, JSBACH employs a flexible land-cover library that allows users to specify the number and properties of PFTs. To reduce uncertainties arising from differences in boundary conditions, the iMAPLE land cover dataset was harmonized and mapped onto the JSBACH PFT categories (Table 1). Comparisons of simulated GPP and LAI from ECHAM6-JSBACH showed improved performance when using the updated PFT derived from iMAPLE (Table 2). Therefore, this updated land cover configuration of ECHAM6-JSBACH is adopted for subsequent comparison with ECHAM6-iMAPLE. We conducted a set of 15-year simulations spanning from 2000 to 2014 to evaluate and compare the performance of ECHAM6-iMAPLE and ECHAM6-JSBACH. The first five years were used for model spin-up, and the remaining ten years were averaged for analysis and performance assessment.

2.4 Data for model evaluations

Observational and reanalysis datasets from 2005 to 2014 were used to evaluate and compare the performance of the ECHAM6-iMAPLE model and ECHAM6-JSBACH

https://doi.org/10.5194/egusphere-2026-1884
Preprint. Discussion started: 26 May 2026

models. Specifically, Global LAnd Surface Satellite (GLASS) products were used to assess LAI. For GPP and ET, we used the benchmark product of FLUXCOM datasets (Tramontana et al., 2016; Jung et al., 2020), which generate global gridded flux estimates using machine learning algorithms trained on flux measurements from FLUXNET eddy covariance sites. We also used the Modern-Era Retrospective analysis for Research and Applications, Version 2 (MERRA-2) product (Gelaro et al., 2017) for the evaluations of soil temperature, soil moisture, surface air temperature, and precipitation. All datasets were interpolated to the T63 spectral resolution for consistent comparisons, corresponding to a horizontal resolution of approximately 1.875° in both latitude and longitude.

3. Results

3.1 Terrestrial carbon cycle

We evaluated the performance of ECHAM6-iMAPLE and ECHAM6-JSBACH in simulating terrestrial carbon fluxes (Fig. 2). Both models reasonably capture the spatial distribution of GPP consistent with FLUXCOM observations, characterized by high values in tropical regions, moderate values in boreal forests, and low values in arid areas. ECHAM6-iMAPLE simulates a global annual total GPP of 126.9 Pg C yr^{-1}, slightly higher than that of 124.1 Pg C yr^{-1} estimated by the FLUXCOM benchmark. In contrast, ECHAM6-JSBACH produces a much higher global GPP of 134.2 Pg C yr^{-1}, with pronounced positive biases mainly over tropical forest regions, including the Indian subcontinent, the Amazon Basin, and Central Africa (Fig. 2c). Relative to ECHAM6-JSBACH, ECHAM6-iMAPLE exhibits improved performance (Fig. 2b), reflected by a higher correlation coefficient ($R = 0.75$, $p < 0.01$) and a lower root mean square error (RMSE = 1.51 g C m^{-2} day^{-1}). This improvement can be primarily attributed to the calibration of vegetation photosynthetic parameters in iMAPLE based on site-level datasets (Yue and Unger, 2015), as well as the constraint of plant phenology through satellite-based observations (Yue et al., 2015).

Consistent with the GPP pattern, simulated LAI from ECHAM6-iMAPLE (Fig. 2e) shows a higher R of 0.86 ($p < 0.01$) and a lower RMSE of 0.73 m^2 m^{-2} against GLASS retrievals (Fig. 2d) compared to ECHAM6-JSBACH (Fig. 2f). Regionally, ECHAM6-iMAPLE successfully reproduces the elevated LAI in tropical rainforests, in good agreement with observational patterns. Globally, ECHAM6-iMAPLE underestimates LAI by about 9%, primarily due to notable underestimation across high-latitude regions

https://doi.org/10.5194/egusphere-2026-1884
Preprint. Discussion started: 26 May 2026

of the Northern Hemisphere (Fig. 2e). In contrast, ECHAM6-JSBACH shows a higher RMSE of 0.79 relative to GLASS, with the largest negative biases occurring in the central Africa and the Southeast Asia region (Fig. 2f).

3.2 Terrestrial water flux

We evaluated the simulated water fluxes from ECHAM6-iMAPLE and ECHAM6-JSBACH (Fig. 3). Both models successfully reproduce the observed ET patterns, characterized by hotspots over tropical rainforest and low values in arid and/or cold regions. Simulated ET from ECHAM6-iMAPLE (Fig. 3b) exhibits a higher spatial correlation with the FLUXCOM benchmark (Fig. 3a) (R=0.86, p<0.01) and a lower RMSE (15.2 mm mon^{-1}) compared to ECHAM6-JSBACH (Fig. 3c). Globally, the area-weighted mean ET simulated by ECHAM6-iMAPLE is 45.5 mm mon^{-1}, closely matching the observed value of 45.9 mm mon^{-1}, whereas ECHAM6-JSBACH underestimates ET at 42.1 mm mon^{-1}. The poorer performance of ECHAM6-JSBACH is mainly attributed to substantial underestimations in arid and semi-arid regions, particularly over the western United States and Australia (Fig. 3c).

For water use efficiency (WUE), defined as the ratio of GPP to ET, ECHAM6-iMAPLE exhibits high values in the northern middle-to-high latitudes and moderate values in the tropics (Fig. 3e). It achieves a spatial R of 0.52 (p < 0.01) and a RMSE of 0.77 g C/kg H_2O against the FLUXCOM benchmark (Fig. 3d). In contrast, ECHAM6-JSBACH exhibits substantially poorer performance, with a lower spatial R of 0.20 and a higher RMSE of 0.95 g C/kg H_2O (Fig. 3f), which is primarily associated with underestimated ET across mid-to-high northern latitudes and Central Africa. At the global scale, the area-weighted mean WUE simulated by ECHAM6-iMAPLE is 1.43 g C/kg H_2O, closer to the FLUXCOM estimate of 1.55 g C/kg H_2O and representing a clear improvement over the 1.35 g C/kg H_2O simulated by ECHAM6-JSBACH (Fig. 3f).

3.3 Seasonal variations

In addition to the spatial pattern, ECHAM6-iMAPLE effectively captures the seasonal cycles of terrestrial carbon and water fluxes (Fig. 4). Consistent with observations, simulated GPP and ET both reach their annual maxima during the vegetation growing season, with the most pronounced peak occurring in July (Figs 3a and 3c). Although the LAI simulated by ECHAM6-iMAPLE exhibits a one-month lag

https://doi.org/10.5194/egusphere-2026-1884
Preprint. Discussion started: 26 May 2026

relative to the observations, the temporal correlation remains high (R=0.96), indicating a good representation of seasonal dynamics (Fig. 4b). In contrast, ECHAM6-JSBACH predicts the annual peaks of terrestrial carbon and water fluxes in June, one month earlier than observed peaks. Moreover, the corresponding R between ECHAM6-JSBACH simulations and observations are consistently lower than those derived from ECHAM6-iMAPLE (Fig. 4). The divergence in peak timing and the systematically lower R values collectively demonstrate that ECHAM6-iMAPLE provides a more accurate representation of the seasonal dynamics of terrestrial carbon and water cycle processes compared to ECHAM6-JSBACH.

3.4 Soil properties and near-surface climate

Soil temperature and moisture play critical roles in regulating vegetation growth (Davidson and Janssens, 2006; Green et al., 2019). Both ECHAM6-iMAPLE (Fig. 5b) and ECHAM6-JSBACH (Fig. 5c) predict high soil temperatures in tropical regions, especially in northern Africa and the Indian Peninsula. The two models exhibit extremely high spatial correlations with MERRA2 reanalysis data (R=0.99 and 0.98, respectively). However, ECHAM6-iMAPLE more accurately reproduces the global mean soil temperature and shows a lower RMSE of 2.16 K, whereas ECHAM6-JSBACH shows a slight warm bias with a higher RMSE of 2.49 K. For soil moisture, ECHAM6-JSBACH shows substantial overestimation in tropical regions and the high-latitude Northern Hemisphere, leading to a 39.1% overestimation of the global mean value compared to MERRA2 (Fig. 5f). In contrast, ECHAM6-iMAPLE closely matches the global mean soil moisture from MERRA2, with a lower RMSE of 0.07 and a moderate spatial R of 0.76 (Fig. 5e).

Changes in soil temperature and moisture influence surface meteorology through land-atmosphere coupling processes (Seneviratne et al., 2006). We therefore compared surface air temperature and precipitation simulated by ECHAM6-iMAPLE and ECHAM6-JSBACH (Fig. 6). Both models reproduce the large-scale spatial distribution of surface air temperature, albeit with overall warm biases (Figs 5b and 5c). However, ECHAM6-iMAPLE performs better than ECHAM6-JSBACH, showing a smaller global mean warm bias (0.34°C vs. 0.76°C) and a lower RMSE (3.33°C vs. 3.47°C). This improvement is likely associated with the more accurate simulation of soil temperature in ECHAM6-iMAPLE (Fig. 5b), highlighting the role of land surface processes in constraining near-surface climate. For precipitation, however, both models

https://doi.org/10.5194/egusphere-2026-1884
Preprint. Discussion started: 26 May 2026

substantially overestimate the global mean amount with regional overestimation in Asia but underestimation in central Africa (Figs 5e and 5f). Although coupling with iMAPLE improves the simulation of ET (Fig. 3b) and soil moisture (Fig. 5e), the complex and nonlinear feedbacks within the hydrological cycle may instead magnify biases in precipitation estimates.

4. Conclusion and Discussion

The terrestrial biosphere and atmosphere are tightly coupled through exchanges of energy, water, carbon, and reactive species (Green et al., 2017). These interactions regulate climate variability, ecosystem resilience, and air pollutants such as ozone and aerosols (Zeng et al., 1999; Yue and Unger, 2014; Zhou et al., 2024). However, climate models often incompletely represent vegetation biophysical and physiological processes, leading to biased carbon and water fluxes and increased uncertainties in weather predictions (Koster et al., 2011; Guo et al., 2012). To address this limitation, we coupled the iMAPLE vegetation model to the ECHAM6 atmospheric general circulation model, and evaluated its performance against reanalysis, benchmark, and satellite datasets. Compared to the original ECHAM6-JSBACH configuration, the updated ECHAM6-iMAPLE model substantially improves simulations of terrestrial carbon and water fluxes, more accurately capturing their spatial patterns and seasonal variations.

These improvements stem from both rigorous parameter calibration and a more realistic representation of key biophysical processes in iMAPLE. Critical physiological parameters (e.g., V_{cmax}) are tightly constrained using *in situ* measurements from 201 FLUXNET sites (Yue et al., 2024), and phenological schemes have been validated against thousands of ground-based records and multiple satellite retrievals (Yue et al., 2015). Moreover, iMAPLE distinguished the biophysical effects of direct and diffuse radiation (Yue and Unger, 2017), allowing improved quantifications of canopy radiation transfer and photosynthetic carbon assimilation dynamics. Unlike JSBACH, which applies a fixed carbon allocation scheme among leaf, wood, and reserve pools, iMAPLE adopts a dynamic framework that allocates carbon to root, stem, and leaf respiration in proportion to realistic LAI variations. Together, these advances enhance the ability of ECHAM6-iMAPLE in simulating vegetation dynamics under climate change.

Despite these advances, several limitations remain in the current version of ECHAM6-iMAPLE. First, iMAPLE does not include dynamic nitrogen and

https://doi.org/10.5194/egusphere-2026-1884
Preprint. Discussion started: 26 May 2026

phosphorus cycles, introducing uncertainties in simulated photosynthetic responses to elevated CO_2 (Gruber and Galloway, 2008; Zaehle et al., 2011). Second, the vegetation model prescribes land cover and neglects competitions among PFTs, preventing simulation of vegetation shifts under anthropogenic or natural disturbances. Third, not all vegetation properties simulated by iMAPLE are fully coupled to ECHAM6. For instance, dynamically simulated LAI is not consistently used by ECHAM6 to update land surface parameters or ecosystem emissions. In addition, iMAPLE considers the variations of soil temperature and soil moisture only within upper two meters, limiting the full prediction of deeper soil processes in the coupled system.

In future work, we will further improve ECHAM6-iMAPLE in several key aspects. First, incorporating a process-based nitrogen cycle will substantially improve simulations of terrestrial carbon sinks and reduce uncertainties in carbon flux estimates. Second, we will strengthen the representation of natural source and sink processes. A major advantage of iMAPLE lies in its dynamic simulation of natural emissions, including wildfires, biogenic volatile organic compounds (BVOCs), and soil emissions. In addition, dynamically simulated stomatal conductance influences the dry deposition of atmospheric constituents. Future efforts will focus on improving the real-time simulation and evaluation of these source-sink processes within the coupled framework. Third, we plan to incorporate an interactive module of atmospheric chemistry into ECHAM6-iMAPLE to enable fully coupled interactions among climate, ecosystems, and atmospheric chemistry. This development will enhance capabilities for climate projection and air pollution forecasting, and provide a useful tool for quantifying of the long-term impacts of human activities on the Earth system through multi-sphere interactions and feedbacks.

Code availability.

The code and model description for ECHAM6-iMAPLE version 1 is available at https://doi.org/10.6084/m9.figshare.31877242 (Fu et al., 2026).

Author contributions.

XY conceived the idea of coupling the two models. WF and CT contributed equally to this work. WF and CT contributed to the coupling process, simulations, and result analysis. YZ, YH, JH, and HC helped with code improvements. All authors contributed to improving the paper.

https://doi.org/10.5194/egusphere-2026-1884
Preprint. Discussion started: 26 May 2026

Financial support.

This study was jointly funded by the National Key Research and Development Program of China (2023YFF0805402) and the National Natural Science Foundation of China (42525503).

Competing interests.

The authors declare that they have no conflict of interest.

Acknowledgments.

The authors thank for the technical support of the National Large Scientific and Technological Infrastructure "Earth System Numerical Simulation Facility" (https://cstr.cn/31134.02.EL).

https://doi.org/10.5194/egusphere-2026-1884
Preprint. Discussion started: 26 May 2026

References

Arakawa, A.: Computational design for long-term numerical integration of the equations of fluid motion: Two-dimensional incompressible flow. Part I, Journal of Computational Physics, 1, 119-143, https://doi.org/10.1016/0021-9991(66)90015-5, 1966.

Arora, V. K., Boer, G. J., Christian, J. R., Curry, C. L., Denman, K. L., Zahariev, K., Flato, G. M., Scinocca, J. F., Merryfield, W. J., and Lee, W. G.: The Effect of Terrestrial Photosynthesis Down Regulation on the Twentieth-Century Carbon Budget Simulated with the CCCma Earth System Model, Journal of Climate, 22, 6066-6088, https://doi.org/10.1175/2009JCLI3037.1, 2009.

Beer, C., Reichstein, M., Tomelleri, E., Ciais, P., Jung, M., Carvalhais, N., Rödenbeck, C., Arain, M. A., Baldocchi, D., Bonan, G. B., Bondeau, A., Cescatti, A., Lasslop, G., Lindroth, A., Lomas, M., Luyssaert, S., Margolis, H., Oleson, K. W., Roupsard, O., Veenendaal, E., Viovy, N., Williams, C., Woodward, F. I., and Papale, D.: Terrestrial Gross Carbon Dioxide Uptake: Global Distribution and Covariation with Climate, Science, 329, 834-838, 10.1126/science.1184984, 2010.

Berg, A., Findell, K., Lintner, B., Giannini, A., Seneviratne, S. I., van den Hurk, B., Lorenz, R., Pitman, A., Hagemann, S., Meier, A., Cheruy, F., Ducharne, A., Malyshev, S., and Milly, P. C. D.: Land–atmosphere feedbacks amplify aridity increase over land under global warming, Nature Climate Change, 6, 869-874, 10.1038/nclimate3029, 2016.

Blyth, E. M., Arora, V. K., Clark, D. B., Dadson, S. J., De Kauwe, M. G., Lawrence, D. M., Melton, J. R., Pongratz, J., Turton, R. H., Yoshimura, K., and Yuan, H.: Advances in Land Surface Modelling, Current Climate Change Reports, 7, 45-71, 10.1007/s40641-021-00171-5, 2021.

Bonan, G. B.: Forests and Climate Change: Forcings, Feedbacks, and the Climate Benefits of Forests, Science, 320, 1444-1449, 10.1126/science.1155121, 2008.

Bourke, W., McAvaney, B., Puri, K., and Thurling, R.: Global Modeling of Atmospheric Flow by Spectral Methods, in: Methods in Computational Physics: Advances in Research and Applications, edited by: Chang, J., Elsevier, 267-324, https://doi.org/10.1016/B978-0-12-460817-7.50010-0, 1977.

Cao, J., Yue, X., and Ma, M.: Simulation of ozone–vegetation coupling and feedback in China using multiple ozone damage schemes, Atmos. Chem. Phys., 24, 3973-3987, 10.5194/acp-24-3973-2024, 2024.

Cao, J., Wang, B., Yang, Y. M., Ma, L., Li, J., Sun, B., Bao, Y., He, J., Zhou, X., and Wu, L.: The NUIST Earth System Model (NESM) version 3: description and preliminary evaluation, Geosci. Model Dev., 11, 2975-2993, 10.5194/gmd-11-2975-2018, 2018.

Collatz, G., Ribas-Carbo, M., and Berry, J.: Coupled Photosynthesis-Stomatal Conductance Model for Leaves of C4 Plants Functional Plant Biology, 19, 519-538, https://doi.org/10.1071/PP9920519, 1992a.

Collatz, G. J., Ribas-Carbó, M., and Berry, J. A. J. A. J. o. P. P.: Coupled Photosynthesis-Stomatal Conductance Model for Leaves of C4 Plants, 19, 519-538, 1992b.

Collatz, G. J., Ball, J. T., Grivet, C., and Berry, J. A.: Physiological and environmental regulation of stomatal conductance, photosynthesis and transpiration: a model that includes a laminar boundary layer, Agricultural and Forest Meteorology, 54, 107-136, https://doi.org/10.1016/0168-1923(91)90002-8, 1991.

Crueger, T., Giorgetta, M. A., Brokopf, R., Esch, M., Fiedler, S., Hohenegger, C., Kornblueh, L., Mauritsen, T., Nam, C., Naumann, A. K., Peters, K., Rast, S., Roeckner, E., Sakradzija, M., Schmidt, H., Vial, J., Vogel, R., and Stevens, B.: ICON-A, The Atmosphere Component of the ICON Earth System Model: II. Model Evaluation, Journal of Advances in Modeling Earth Systems, 10, 1638-1662, https://doi.org/10.1029/2017MS001233, 2018.

Dalmonech, D. and Zaehle, S.: Towards a more objective evaluation of modelled land-carbon trends using atmospheric CO_2 and satellite-based vegetation activity observations, Biogeosciences, 10, 4189-4210, 10.5194/bg-10-4189-2013, 2013.

Dalmonech, D., Zaehle, S., Schürmann, G. J., Brovkin, V., Reick, C., and Schnur, R.: Separation of the Effects of Land and Climate Model Errors on Simulated Contemporary Land Carbon

https://doi.org/10.5194/egusphere-2026-1884
Preprint. Discussion started: 26 May 2026

Cycle Trends in the MPI Earth System Model version 1, Journal of Climate, 28, 272-291, https://doi.org/10.1175/JCLI-D-13-00593.1, 2015.
Davidson, E. A. and Janssens, I. A.: Temperature sensitivity of soil carbon decomposition and feedbacks to climate change, Nature, 440, 165-173, 10.1038/nature04514, 2006.
Defries, R. S., Hansen, M. C., Townshend, J. R. G., Janetos, A. C., and Loveland, T. R.: A new global 1-km dataset of percentage tree cover derived from remote sensing, Global Change Biology, 6, 247-254, https://doi.org/10.1046/j.1365-2486.2000.00296.x, 2000.
Dickinson, R. E.: Land Surface Processes and Climate—Surface Albedos and Energy Balance, in: Advances in Geophysics, edited by: Saltzman, B., Elsevier, 305-353, https://doi.org/10.1016/S0065-2687(08)60176-4, 1983.
Farquhar, G. D., von Caemmerer, S., and Berry, J. A.: A biochemical model of photosynthetic CO2 assimilation in leaves of C3 species, Planta, 149, 78-90, 10.1007/BF00386231, 1980.
Fastovich, D., Meyers, S. R., Saupe, E. E., Williams, J. W., Dornelas, M., Dowding, E. M., Finnegan, S., Huang, H.-H. M., Jonkers, L., Kiessling, W., Kocsis, Á. T., Li, Q., Liow, L. H., Na, L., Penny, A. M., Pippenger, K., Renaudie, J., Rillo, M. C., Smith, J., Steinbauer, M. J., Sugawara, M., Tomašových, A., Yasuhara, M., and Hull, P. M.: Coupled, decoupled, and abrupt responses of vegetation to climate across timescales, Science, 389, 64-68, 10.1126/science.adr6700, 2025.
Fisher, R. A. and Koven, C. D.: Perspectives on the Future of Land Surface Models and the Challenges of Representing Complex Terrestrial Systems, Journal of Advances in Modeling Earth Systems, 12, e2018MS001453, https://doi.org/10.1029/2018MS001453, 2020.
Forzieri, G., Miralles, D. G., Ciais, P., Alkama, R., Ryu, Y., Duveiller, G., Zhang, K., Robertson, E., Kautz, M., Martens, B., Jiang, C., Arneth, A., Georgievski, G., Li, W., Ceccherini, G., Anthoni, P., Lawrence, P., Wiltshire, A., Pongratz, J., Piao, S., Sitch, S., Goll, D. S., Arora, V. K., Lienert, S., Lombardozzi, D., Kato, E., Nabel, J. E. M. S., Tian, H., Friedlingstein, P., and Cescatti, A.: Increased control of vegetation on global terrestrial energy fluxes, Nature Climate Change, 10, 356-362, 10.1038/s41558-020-0717-0, 2020.
Friedlingstein, P., O'Sullivan, M., Jones, M. W., Andrew, R. M., Hauck, J., Landschützer, P., Le Quéré, C., Li, H., Luijkx, I. T., Olsen, A., Peters, G. P., Peters, W., Pongratz, J., Schwingshackl, C., Sitch, S., Canadell, J. G., Ciais, P., Jackson, R. B., Alin, S. R., Arneth, A., Arora, V., Bates, N. R., Becker, M., Bellouin, N., Berghoff, C. F., Bittig, H. C., Bopp, L., Cadule, P., Campbell, K., Chamberlain, M. A., Chandra, N., Chevallier, F., Chini, L. P., Colligan, T., Decayeux, J., Djeutchouang, L. M., Dou, X., Duran Rojas, C., Enyo, K., Evans, W., Fay, A. R., Feely, R. A., Ford, D. J., Foster, A., Gasser, T., Gehlen, M., Gkritzalis, T., Grassi, G., Gregor, L., Gruber, N., Gürses, Ö., Harris, I., Hefner, M., Heinke, J., Hurtt, G. C., Iida, Y., Ilyina, T., Jacobson, A. R., Jain, A. K., Jarníková, T., Jersild, A., Jiang, F., Jin, Z., Kato, E., Keeling, R. F., Klein Goldewijk, K., Knauer, J., Korsbakken, J. I., Lan, X., Lauvset, S. K., Lefèvre, N., Liu, Z., Liu, J., Ma, L., Maksyutov, S., Marland, G., Mayot, N., McGuire, P. C., Metzl, N., Monacci, N. M., Morgan, E. J., Nakaoka, S. I., Neill, C., Niwa, Y., Nützel, T., Olivier, L., Ono, T., Palmer, P. I., Pierrot, D., Qin, Z., Resplandy, L., Roobaert, A., Rosan, T. M., Rödenbeck, C., Schwinger, J., Smallman, T. L., Smith, S. M., Sospedra-Alfonso, R., Steinhoff, T., Sun, Q., Sutton, A. J., Séférian, R., Takao, S., Tatebe, H., Tian, H., Tilbrook, B., Torres, O., Tourigny, E., Tsujino, H., Tubiello, F., van der Werf, G., Wanninkhof, R., Wang, X., Yang, D., Yang, X., Yu, Z., Yuan, W., Yue, X., Zaehle, S., Zeng, N., and Zeng, J.: Global Carbon Budget 2024, Earth Syst. Sci. Data, 17, 965-1039, 10.5194/essd-17-965-2025, 2025.
Fu, W., Tian, C., and Yue, X.: ECHAM6-iMAPLE v1.0 coupled atmosphere-ecosystem model, figshare [code], 10.6084/m9.figshare.31877242.v1, 2026.
Gelaro, R., McCarty, W., Suárez, M. J., Todling, R., Molod, A., Takacs, L., Randles, C. A., Darmenov, A., Bosilovich, M. G., Reichle, R., Wargan, K., Coy, L., Cullather, R., Draper, C., Akella, S., Buchard, V., Conaty, A., da Silva, A. M., Gu, W., Kim, G.-K., Koster, R., Lucchesi, R., Merkova, D., Nielsen, J. E., Partyka, G., Pawson, S., Putman, W., Rienecker, M., Schubert, S. D., Sienkiewicz, M., and Zhao, B.: The Modern-Era Retrospective Analysis for Research and Applications, Version 2 (MERRA-2), Journal of Climate, 30, 5419-5454, https://doi.org/10.1175/JCLI-D-16-0758.1, 2017.

https://doi.org/10.5194/egusphere-2026-1884
Preprint. Discussion started: 26 May 2026

Giorgetta, M., Roeckner, E., Mauritsen, T., Bader, J., Crueger, T., Esch, M., Rast, S., Kornblueh, L., Schmidt, H., Kinne, S., Hohenegger, C., Möbis, B., Krismer, T., Wieners, K.-H., and Stevens, B.: The atmospheric general circulation model ECHAM6 - Model description, 10.17617/2.1810480, 2013.

Goll, D. S., Winkler, A. J., Raddatz, T., Dong, N., Prentice, I. C., Ciais, P., and Brovkin, V.: Carbon–nitrogen interactions in idealized simulations with JSBACH (version 3.10), Geosci. Model Dev., 10, 2009-2030, 10.5194/gmd-10-2009-2017, 2017.

Green, J. K., Seneviratne, S. I., Berg, A. M., Findell, K. L., Hagemann, S., Lawrence, D. M., and Gentine, P.: Large influence of soil moisture on long-term terrestrial carbon uptake, Nature, 565, 476-479, 10.1038/s41586-018-0848-x, 2019.

Green, J. K., Konings, A. G., Alemohammad, S. H., Berry, J., Entekhabi, D., Kolassa, J., Lee, J.-E., and Gentine, P.: Regionally strong feedbacks between the atmosphere and terrestrial biosphere, Nature Geoscience, 10, 410-414, 10.1038/ngeo2957, 2017.

Gruber, N. and Galloway, J. N.: An Earth-system perspective of the global nitrogen cycle, Nature, 451, 293-296, 10.1038/nature06592, 2008.

Gulden, L. E., Yang, Z.-L., and Niu, G.-Y.: Interannual variation in biogenic emissions on a regional scale, Journal of Geophysical Research: Atmospheres, 112, https://doi.org/10.1029/2006JD008231, 2007.

Guo, Z., Dirmeyer, P. A., DelSole, T., and Koster, R. D.: Rebound in Atmospheric Predictability and the Role of the Land Surface, Journal of Climate, 25, 4744-4749, https://doi.org/10.1175/JCLI-D-11-00651.1, 2012.

Hagemann, S. and Stacke, T.: Impact of the soil hydrology scheme on simulated soil moisture memory, Climate Dynamics, 44, 1731-1750, 10.1007/s00382-014-2221-6, 2015.

Hansen, M. C., DeFries, R. S., Townshend, J. R. G., Carroll, M., Dimiceli, C., and Sohlberg, R. A.: Global Percent Tree Cover at a Spatial Resolution of 500 Meters: First Results of the MODIS Vegetation Continuous Fields Algorithm, Earth Interactions, 7, 1-15, https://doi.org/10.1175/1087-3562(2003)007<0001:GPTCAA>2.0.CO;2, 2003.

Heimann, M. and Reichstein, M.: Terrestrial ecosystem carbon dynamics and climate feedbacks, Nature, 451, 289-292, 10.1038/nature06591, 2008.

Higgins, S. I., Conradi, T., and Muhoko, E.: Shifts in vegetation activity of terrestrial ecosystems attributable to climate trends, Nature Geoscience, 16, 147-153, 10.1038/s41561-022-01114-x, 2023.

Jung, M., Schwalm, C., Migliavacca, M., Walther, S., Camps-Valls, G., Koirala, S., Anthoni, P., Besnard, S., Bodesheim, P., Carvalhais, N., Chevallier, F., Gans, F., Goll, D. S., Haverd, V., Köhler, P., Ichii, K., Jain, A. K., Liu, J., Lombardozzi, D., Nabel, J. E. M. S., Nelson, J. A., O'Sullivan, M., Pallandt, M., Papale, D., Peters, W., Pongratz, J., Rödenbeck, C., Sitch, S., Tramontana, G., Walker, A., Weber, U., and Reichstein, M.: Scaling carbon fluxes from eddy covariance sites to globe: synthesis and evaluation of the FLUXCOM approach, Biogeosciences, 17, 1343-1365, 10.5194/bg-17-1343-2020, 2020.

Knorr, W.: Annual and interannual CO_2 exchanges of the terrestrial biosphere: process-based simulations and uncertainties, Global Ecology and Biogeography, 9, 225-252, https://doi.org/10.1046/j.1365-2699.2000.00159.x, 2000.

Koster, R. D., Mahanama, S. P. P., Yamada, T. J., Balsamo, G., Berg, A. A., Boisserie, M., Dirmeyer, P. A., Doblas-Reyes, F. J., Drewitt, G., Gordon, C. T., Guo, Z., Jeong, J. H., Lee, W. S., Li, Z., Luo, L., Malyshev, S., Merryfield, W. J., Seneviratne, S. I., Stanelle, T., van den Hurk, B. J. J. M., Vitart, F., and Wood, E. F.: The Second Phase of the Global Land–Atmosphere Coupling Experiment: Soil Moisture Contributions to Subseasonal Forecast Skill, Journal of Hydrometeorology, 12, 805-822, https://doi.org/10.1175/2011JHM1365.1, 2011.

Kretzschmar, J., Salzmann, M., Mülmenstädt, J., and Quaas, J.: Arctic clouds in ECHAM6 and their sensitivity to cloud microphysics and surface fluxes, Atmos. Chem. Phys., 19, 10571-10589, 10.5194/acp-19-10571-2019, 2019.

Lawrence, D. M., Oleson, K. W., Flanner, M. G., Thornton, P. E., Swenson, S. C., Lawrence, P. J., Zeng, X., Yang, Z.-L., Levis, S., Sakaguchi, K., Bonan, G. B., and Slater, A. G.: Parameterization improvements and functional and structural advances in Version 4 of the

https://doi.org/10.5194/egusphere-2026-1884
Preprint. Discussion started: 26 May 2026

Community Land Model, Journal of Advances in Modeling Earth Systems, 3, https://doi.org/10.1029/2011MS00045, 2011.
Li, F., Zeng, X. D., and Levis, S.: A process-based fire parameterization of intermediate complexity in a Dynamic Global Vegetation Model, Biogeosciences, 9, 2761-2780, 10.5194/bg-9-2761-2012, 2012.
Meador, W. E. and Weaver, W. R.: Two-Stream Approximations to Radiative Transfer in Planetary Atmospheres: A Unified Description of Existing Methods and a New Improvement, Journal of Atmospheric Sciences, 37, 630-643, https://doi.org/10.1175/1520-0469(1980)037<0630:TSATRT>2.0.CO;2, 1980.
Niu, G.-Y., Yang, Z.-L., Mitchell, K. E., Chen, F., Ek, M. B., Barlage, M., Kumar, A., Manning, K., Niyogi, D., Rosero, E., Tewari, M., and Xia, Y.: The community Noah land surface model with multiparameterization options (Noah-MP): 1. Model description and evaluation with local-scale measurements, Journal of Geophysical Research: Atmospheres, 116, https://doi.org/10.1029/2010JD015139, 2011.
Nolan, C., Overpeck, J. T., Allen, J. R. M., Anderson, P. M., Betancourt, J. L., Binney, H. A., Brewer, S., Bush, M. B., Chase, B. M., Cheddadi, R., Djamali, M., Dodson, J., Edwards, M. E., Gosling, W. D., Haberle, S., Hotchkiss, S. C., Huntley, B., Ivory, S. J., Kershaw, A. P., Kim, S.-H., Latorre, C., Leydet, M., Lézine, A.-M., Liu, K.-B., Liu, Y., Lozhkin, A. V., McGlone, M. S., Marchant, R. A., Momohara, A., Moreno, P. I., Müller, S., Otto-Bliesner, B. L., Shen, C., Stevenson, J., Takahara, H., Tarasov, P. E., Tipton, J., Vincens, A., Weng, C., Xu, Q., Zheng, Z., and Jackson, S. T.: Past and future global transformation of terrestrial ecosystems under climate change, Science, 361, 920-923, 10.1126/science.aan5360, 2018.
Parmesan, C. and Yohe, G.: A globally coherent fingerprint of climate change impacts across natural systems, Nature, 421, 37-42, 10.1038/nature01286, 2003.
Pechony, O. and Shindell, D. T.: Fire parameterization on a global scale, Journal of Geophysical Research: Atmospheres, 114, https://doi.org/10.1029/2009JD011927, 2009.
Phillips, N. A.: A COORDINATE SYSTEM HAVING SOME SPECIAL ADVANTAGES FOR NUMERICAL FORECASTING, Journal of Atmospheric Sciences, 14, 184-185, https://doi.org/10.1175/1520-0469(1957)014<0184:ACSHSS>2.0.CO;2, 1957.
Pielke, R. A., Sr, Avissar, R., Raupach, M., Dolman, A. J., Zeng, X., and Denning, A. S.: Interactions between the atmosphere and terrestrial ecosystems: influence on weather and climate, Global Change Biology, 4, 461-475, https://doi.org/10.1046/j.1365-2486.1998.t01-1-00176.x, 1998.
Pitman, A. J.: The evolution of, and revolution in, land surface schemes designed for climate models, International Journal of Climatology, 23, 479-510, https://doi.org/10.1002/joc.893, 2003.
Reick, C. H., Raddatz, T., Brovkin, V., and Gayler, V.: Representation of natural and anthropogenic land cover change in MPI-ESM, Journal of Advances in Modeling Earth Systems, 5, 459-482, https://doi.org/10.1002/jame.20022, 2013.
Richards, L. A.: CAPILLARY CONDUCTION OF LIQUIDS THROUGH POROUS MEDIUMS, Physics, 1, 318-333, 10.1063/1.1745010 %J Physics, 1931.
Ruehr, S., Keenan, T. F., Williams, C., Zhou, Y., Lu, X., Bastos, A., Canadell, J. G., Prentice, I. C., Sitch, S., and Terrer, C.: Evidence and attribution of the enhanced land carbon sink, Nature Reviews Earth & Environment, 4, 518-534, 10.1038/s43017-023-00456-3, 2023.
Schumacher, D. L., Keune, J., Dirmeyer, P., and Miralles, D. G.: Drought self-propagation in drylands due to land–atmosphere feedbacks, Nature Geoscience, 15, 262-268, 10.1038/s41561-022-00912-7, 2022.
Seidl, R., Thom, D., Kautz, M., Martin-Benito, D., Peltoniemi, M., Vacchiano, G., Wild, J., Ascoli, D., Petr, M., Honkaniemi, J., Lexer, M. J., Trotsiuk, V., Mairota, P., Svoboda, M., Fabrika, M., Nagel, T. A., and Reyer, C. P. O.: Forest disturbances under climate change, Nature Climate Change, 7, 395-402, 10.1038/nclimate3303, 2017.
Sellers, P. J., Berry, J. A., Collatz, G. J., Field, C. B., and Hall, F. G.: Canopy reflectance, photosynthesis, and transpiration. III. A reanalysis using improved leaf models and a new canopy integration scheme, Remote Sensing of Environment, 42, 187-216, https://doi.org/10.1016/0034-4257(92)90102-P, 1992.

https://doi.org/10.5194/egusphere-2026-1884
Preprint. Discussion started: 26 May 2026

Sellers, P. J., Dickinson, R. E., Randall, D. A., Betts, A. K., Hall, F. G., Berry, J. A., Collatz, G. J., Denning, A. S., Mooney, H. A., Nobre, C. A., Sato, N., Field, C. B., and Henderson-Sellers, A.: Modeling the Exchanges of Energy, Water, and Carbon Between Continents and the Atmosphere, Science, 275, 502-509, 10.1126/science.275.5299.502, 1997.

Seneviratne, S. I., Lüthi, D., Litschi, M., and Schär, C.: Land–atmosphere coupling and climate change in Europe, Nature, 443, 205-209, 10.1038/nature05095, 2006.

Sidorenko, D., Rackow, T., Jung, T., Semmler, T., Barbi, D., Danilov, S., Dethloff, K., Dorn, W., Fieg, K., Goessling, H. F., Handorf, D., Harig, S., Hiller, W., Juricke, S., Losch, M., Schröter, J., Sein, D. V., and Wang, Q.: Towards multi-resolution global climate modeling with ECHAM6–FESOM. Part I: model formulation and mean climate, Climate Dynamics, 44, 757-780, 10.1007/s00382-014-2290-6, 2015.

Simmons, A. J. and Burridge, D. M.: An Energy and Angular-Momentum Conserving Vertical Finite-Difference Scheme and Hybrid Vertical Coordinates, Monthly Weather Review, 109, 758-766, https://doi.org/10.1175/1520-0493(1981)109<0758:AEAAMC>2.0.CO;2, 1981.

Siongco, A. C., Hohenegger, C., and Stevens, B.: Sensitivity of the summertime tropical Atlantic precipitation distribution to convective parameterization and model resolution in ECHAM6, Journal of Geophysical Research: Atmospheres, 122, 2579-2594, https://doi.org/10.1002/2016JD026093, 2017.

Sitch, S., Cox, P. M., Collins, W. J., and Huntingford, C.: Indirect radiative forcing of climate change through ozone effects on the land-carbon sink, Nature, 448, 791-794, 10.1038/nature06059, 2007.

Spitters, C. J. T.: Separating the diffuse and direct component of global radiation and its implications for modeling canopy photosynthesis Part II. Calculation of canopy photosynthesis, Agricultural and Forest Meteorology, 38, 231-242, https://doi.org/10.1016/0168-1923(86)90061-4, 1986.

Spitters, C. J. T., Toussaint, H. A. J. M., and Goudriaan, J.: Separating the diffuse and direct component of global radiation and its implications for modeling canopy photosynthesis Part I. Components of incoming radiation, Agricultural and Forest Meteorology, 38, 217-229, https://doi.org/10.1016/0168-1923(86)90060-2, 1986.

Stevens, B., Giorgetta, M., Esch, M., Mauritsen, T., Crueger, T., Rast, S., Salzmann, M., Schmidt, H., Bader, J., Block, K., Brokopf, R., Fast, I., Kinne, S., Kornblueh, L., Lohmann, U., Pincus, R., Reichler, T., and Roeckner, E.: Atmospheric component of the MPI-M Earth System Model: ECHAM6, Journal of Advances in Modeling Earth Systems, 5, 146-172, https://doi.org/10.1002/jame.20015, 2013.

Stier, P., Feichter, J., Kinne, S., Kloster, S., Vignati, E., Wilson, J., Ganzeveld, L., Tegen, I., Werner, M., Balkanski, Y., Schulz, M., Boucher, O., Minikin, A., and Petzold, A.: The aerosol-climate model ECHAM5-HAM, Atmos. Chem. Phys., 5, 1125-1156, 10.5194/acp-5-1125-2005, 2005.

Tegen, I., Neubauer, D., Ferrachat, S., Siegenthaler-Le Drian, C., Bey, I., Schutgens, N., Stier, P., Watson-Parris, D., Stanelle, T., Schmidt, H., Rast, S., Kokkola, H., Schultz, M., Schroeder, S., Daskalakis, N., Barthel, S., Heinold, B., and Lohmann, U.: The global aerosol–climate model ECHAM6.3–HAM2.3 – Part 1: Aerosol evaluation, Geosci. Model Dev., 12, 1643-1677, 10.5194/gmd-12-1643-2019, 2019.

Todini, E.: The ARNO rainfall—runoff model, Journal of Hydrology, 175, 339-382, https://doi.org/10.1016/S0022-1694(96)80016-3, 1996.

Tramontana, G., Jung, M., Schwalm, C. R., Ichii, K., Camps-Valls, G., Ráduly, B., Reichstein, M., Arain, M. A., Cescatti, A., Kiely, G., Merbold, L., Serrano-Ortiz, P., Sickert, S., Wolf, S., and Papale, D.: Predicting carbon dioxide and energy fluxes across global FLUXNET sites with regression algorithms, Biogeosciences, 13, 4291-4313, 10.5194/bg-13-4291-2016, 2016.

von Caemmerer, S. and Farquhar, G. D.: Some relationships between the biochemistry of photosynthesis and the gas exchange of leaves, Planta, 153, 376-387, 10.1007/BF00384257, 1981.

Walter, B. P., Heimann, M., and Matthews, E.: Modeling modern methane emissions from natural wetlands: 1. Model description and results, Journal of Geophysical Research: Atmospheres, 106, 34189-34206, https://doi.org/10.1029/2001JD900165, 2001.

https://doi.org/10.5194/egusphere-2026-1884
Preprint. Discussion started: 26 May 2026

Wei, J., Dirmeyer, P. A., Yang, Z.-L., and Chen, H.: Effect of land model ensemble versus coupled model ensemble on the simulation of precipitation climatology and variability, Theoretical and Applied Climatology, 134, 793-800, 10.1007/s00704-017-2310-7, 2018.

Wei, J., Dirmeyer, P. A., Guo, Z., Zhang, L., and Misra, V.: How Much Do Different Land Models Matter for Climate Simulation? Part I: Climatology and Variability, Journal of Climate, 23, 3120-3134, https://doi.org/10.1175/2010JCLI3177.1, 2010.

Williams, I. N. and Torn, M. S.: Vegetation controls on surface heat flux partitioning, and land-atmosphere coupling, Geophysical Research Letters, 42, 9416-9424, https://doi.org/10.1002/2015GL066305, 2015.

Yue, X. and Unger, N.: Ozone vegetation damage effects on gross primary productivity in the United States, Atmos. Chem. Phys., 14, 9137-9153, 10.5194/acp-14-9137-2014, 2014.

Yue, X. and Unger, N.: The Yale Interactive terrestrial Biosphere model version 1.0: description, evaluation and implementation into NASA GISS ModelE2, Geosci. Model Dev., 8, 2399-2417, 10.5194/gmd-8-2399-2015, 2015.

Yue, X. and Unger, N.: Aerosol optical depth thresholds as a tool to assess diffuse radiation fertilization of the land carbon uptake in China, Atmos. Chem. Phys., 17, 1329-1342, 10.5194/acp-17-1329-2017, 2017.

Yue, X., Unger, N., Keenan, T. F., Zhang, X., and Vogel, C. S.: Probing the past 30-year phenology trend of US deciduous forests, Biogeosciences, 12, 4693-4709, 10.5194/bg-12-4693-2015, 2015.

Yue, X., Zhou, H., Tian, C., Ma, Y., Hu, Y., Gong, C., Zheng, H., and Liao, H.: Development and evaluation of the interactive Model for Air Pollution and Land Ecosystems (iMAPLE) version 1.0, Geosci. Model Dev., 17, 4621-4642, 10.5194/gmd-17-4621-2024, 2024.

Zaehle, S., Ciais, P., Friend, A. D., and Prieur, V.: Carbon benefits of anthropogenic reactive nitrogen offset by nitrous oxide emissions, Nature Geoscience, 4, 601-605, 10.1038/ngeo1207, 2011.

Zeng, N., Neelin, J. D., Lau, K. M., and Tucker, C. J.: Enhancement of Interdecadal Climate Variability in the Sahel by Vegetation Interaction, Science, 286, 1537-1540, 10.1126/science.286.5444.1537, 1999.

Zeng, Z., Piao, S., Li, L. Z. X., Zhou, L., Ciais, P., Wang, T., Li, Y., Lian, X., Wood, E. F., Friedlingstein, P., Mao, J., Estes, L. D., Myneni, Ranga B., Peng, S., Shi, X., Seneviratne, S. I., and Wang, Y.: Climate mitigation from vegetation biophysical feedbacks during the past three decades, Nature Climate Change, 7, 432-436, 10.1038/nclimate3299, 2017.

Zhang, K., Zuo, Z., Mei, W., Zhang, R., and Dai, A.: A westward shift of heatwave hotspots caused by warming-enhanced land–air coupling, Nature Climate Change, 15, 546-553, 10.1038/s41558-025-02302-4, 2025.

Zhou, H., Yue, X., Dai, H., Geng, G., Yuan, W., Chen, J., Shen, G., Zhang, T., Zhu, J., and Liao, H.: Recovery of ecosystem productivity in China due to the Clean Air Action plan, Nature Geoscience, 17, 1233-1239, 10.1038/s41561-024-01586-z, 2024.

Zhou, S., Williams, A. P., Lintner, B. R., Berg, A. M., Zhang, Y., Keenan, T. F., Cook, B. I., Hagemann, S., Seneviratne, S. I., and Gentine, P.: Soil moisture–atmosphere feedbacks mitigate declining water availability in drylands, Nature Climate Change, 11, 38-44, 10.1038/s41558-020-00945-z, 2021.

Zhu, Q., Liu, J., Peng, C., Chen, H., Fang, X., Jiang, H., Yang, G., Zhu, D., Wang, W., and Zhou, X.: Modelling methane emissions from natural wetlands by development and application of the TRIPLEX-GHG model, Geosci. Model Dev., 7, 981-999, 10.5194/gmd-7-981-2014, 2014.

https://doi.org/10.5194/egusphere-2026-1884
Preprint. Discussion started: 26 May 2026

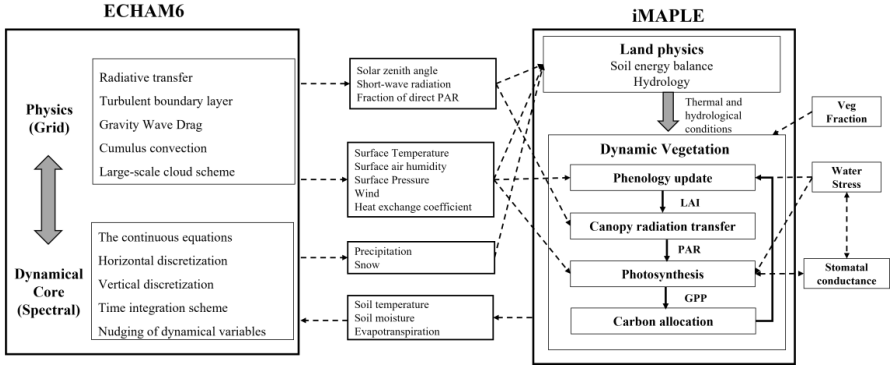

Figure 1. The integrated modeling framework for ECHAM6-iMAPLE v1.0: Atmosphere-Ecosystem Coupled Model.

https://doi.org/10.5194/egusphere-2026-1884
Preprint. Discussion started: 26 May 2026

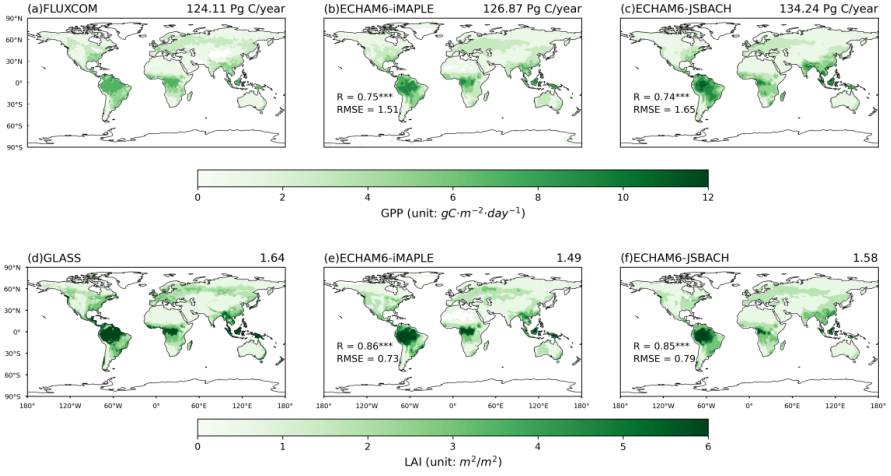

Figure 2. Spatial distributions of (a) gross primary productivity (GPP, g Cm^{-2} day^{-1}) from FLUXCOM and (d) leaf area index (LAI, m^2/m^2) from GLASS, compared with simulations from (b, e) ECHAM6-iMAPLE and (c, f) ECHAM6-JSBACH. Both model simulations and benchmark/observational datasets are averaged for the period of 2005-2014. The spatial correlation coefficient (R) and root mean square errors (RMSE) between simulations and the corresponding observations are shown in the lower left corner of the simulation panels.

https://doi.org/10.5194/egusphere-2026-1884
Preprint. Discussion started: 26 May 2026

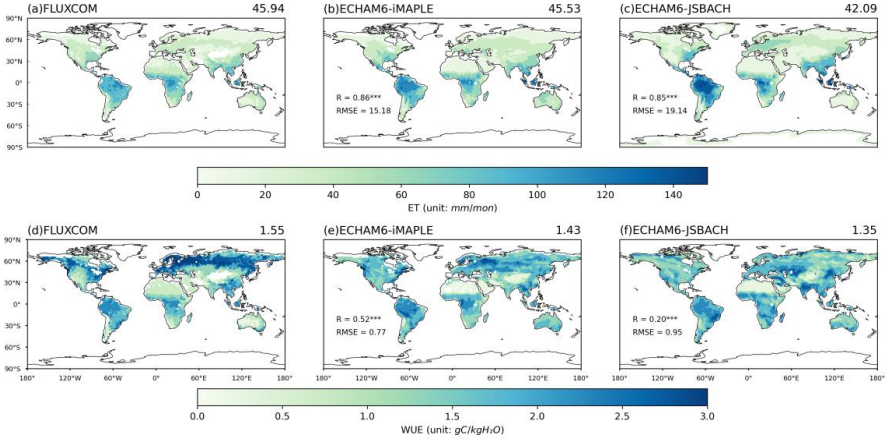

Figure 3. Spatial distributions of (a) evapotranspiration (ET, mm/mon) and (d) water use efficiency (WUE, g C/kg H_2O) from FLUXCOM, compared with simulations from (b, e) ECHAM6-iMAPLE and (c, f) ECHAM6-JSBACH. Both model simulations and the FLUXCOM benchmark datasets are averaged for the period of 2005-2014. The spatial R and RMSE between simulations and benchmark are shown in the lower left corner of simulation panels. The area-weighted mean ET and WUE are indicated at the top of each panel.

https://doi.org/10.5194/egusphere-2026-1884
Preprint. Discussion started: 26 May 2026

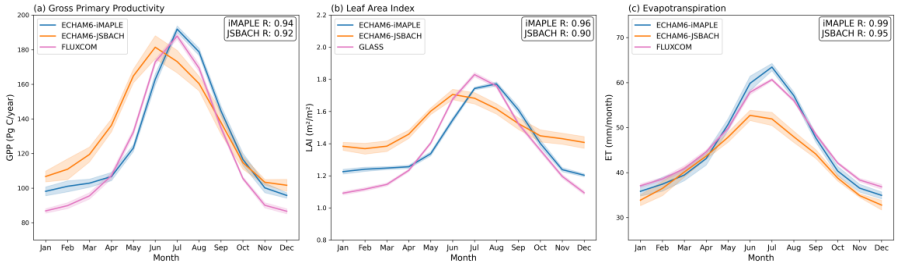

Figure 4. Comparison of the seasonal cycle of (a) GPP (Pg C/year), (b) LAI (m^2/m^2), (c) ET (mm/mon) (c). The pink lines represent observational or benchmark datasets. The blue and orange lines represent simulations from the ECHAM6-iMAPLE and ECHAM6-JSBACH models, respectively. The shaded areas indicate the interannual variability (one standard deviation) over the period 2005-2014.

https://doi.org/10.5194/egusphere-2026-1884
Preprint. Discussion started: 26 May 2026

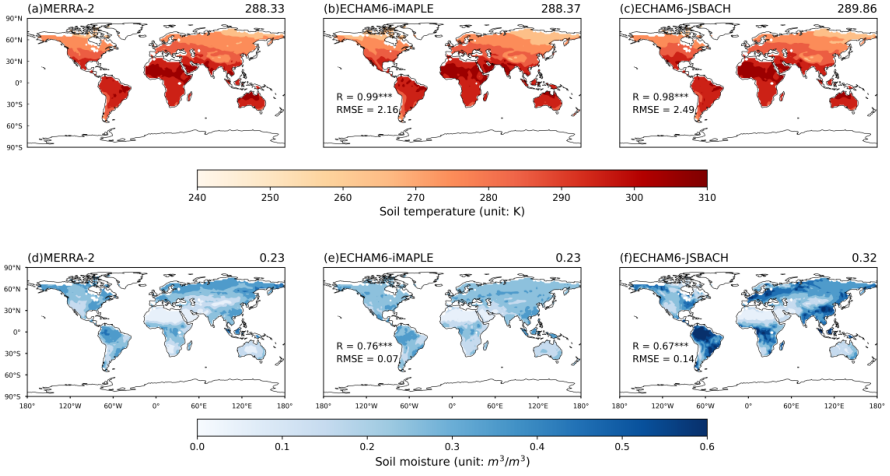

Figure 5. Spatial distributions of (a) soil temperature (ST, K) and (d) soil moisture (SM, m^3/m^3) from MERRA2 reanalyses, compared with simulations from (b, e) ECHAM6-iMAPLE and (c, f) ECHAM6-JSBACH. Both model simulations and MERRA2 reanalyses are averaged for the period of 2005-2014. The spatial R and RMSE between simulations and reanalyses are shown in the lower left corner of simulation panels. The area-weighted mean ST and SM are indicated at the top of each panel.

https://doi.org/10.5194/egusphere-2026-1884
Preprint. Discussion started: 26 May 2026

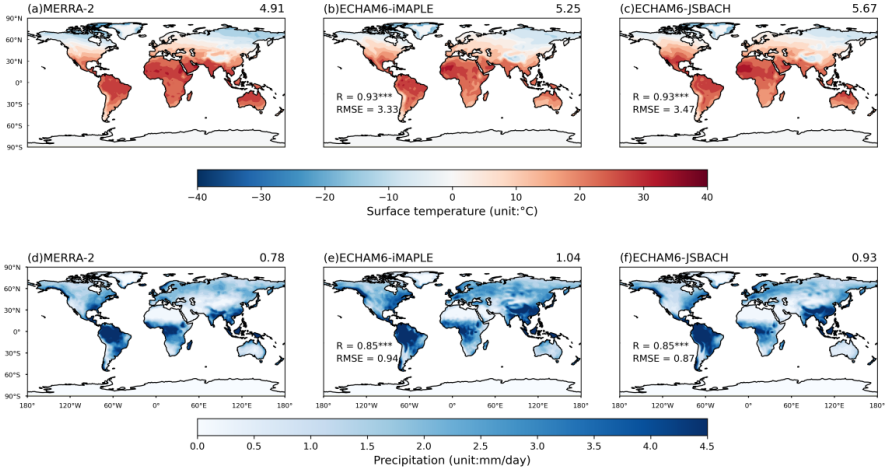

Figure 6. Spatial distributions of (a) surface temperature (T, °C) and (d) precipitation (PREC, mm/day) from MERRA2 reanalyses, compared with simulations from (b, e) ECHAM6-iMAPLE and (c, f) ECHAM6-JSBACH. Both model simulations and MERRA2 reanalyses are averaged for the period of 2005-2014. The spatial R and RMSE between simulations and observations are shown in the lower left corner of simulation panels. The area-weighted mean T and PREC are indicated at the top of each panel.

https://doi.org/10.5194/egusphere-2026-1884
Preprint. Discussion started: 26 May 2026

852 **Table 1** Projection of PFTs from JSBACH to iMAPLE

JSBACH	iMAPLE
Glacier and Tropical evergreen trees	evergreen broadleaf
Tropical deciduous trees	
Extra-tropical evergreen trees	evergreen needleleaf
Extra-tropical evergreen trees	deciduous broadleaf
Raingreen shrubs	arid adapted shrub
Deciduous shrubs	cold shrub
C_3 grass and pasture	C_3 grass
C_4 grass and pasture	C_4 grass
C_3 crop	C_3 crop
C_4 crop	C_4 crop

853
854

https://doi.org/10.5194/egusphere-2026-1884
Preprint. Discussion started: 26 May 2026

Table 2 Comparison of Gross Primary Productivity (GPP) and Leaf Area Index (LAI) between observational datasets and simulations from ECHAM6-iMAPLE and ECHAM6-JSBACH with original/updated PFTs.

	GPP (Pg C/year)	LAI (m^2/m^2)
Observation	124.11	1.64
ECHAM6-iMAPLE	126.87	1.49
ECHAM6-JSBACH (original PFTs)	142.13	1.56
ECHAM6-JSBACH (updated PFTs)	134.24	1.58